ELSEVIER

Journal of Power Sources 92 (2001) 88–94

JOURNAL OF POWER SOURCES

www.elsevier.com/locate/jpowsour

# Catalytic activity of Ni–YSZ–$CeO_2$ anode for the steam reforming of methane in a direct internal-reforming solid oxide fuel cell

Nobuyoshi Nakagawa*, Hitoei Sagara, Kunio Kato

*Department of Biological and Chemical Engineering, Gunma University, 1-5-1 Tenjin, Kiryu, Gunma 376-8515, Japan*

Received 24 August 1999; received in revised form 10 April 2000; accepted 20 May 2000

**Abstract**

As one of the key technologies in the development of a direct internal-reforming solid oxide fuel cell, catalytic activity and stability of a Ni–YSZ–$CeO_2$ anode on a zirconia electrolyte for the steam reforming of methane was investigated by experiments using a differential fuel cell reactor. The effects of the partial pressure of $CH_4$, $H_2O$ and $H_2$, and temperature as well as the electrochemical oxidation on the catalytic activity were analyzed. It was found that the catalytic activity of the Ni–YSZ–$CeO_2$ anode was higher than that of the Ni–YSZ reported especially at low temperature. A deterioration of the catalytic activity of the anode was observed at low $P_{H_2}$ and high $P_{H_2O}$ atmosphere, and also at high current densities. This might be caused by the oxidation of the Ni surface by $H_2O$ in the reaction gas and that produced by the anodic reaction. A rate equation for a fractional function for the steam reforming on open circuit was also proposed.


*Keywords:* Solid oxide fuel cell; Internal-reforming; Steam reforming of methane; Ni–YSZ–$CeO_2$ catalyst; Zirconia electrolyte; Electrochemical oxidation of hydrogen

## 1. Introduction

Solid oxide fuel cells (SOFCs) operated at high temperatures over 1000 K are attractive power generation processes that convert the chemical energy of fuel to electricity efficiently without the restriction of Carnot's law. In addition to the high efficiency of the SOFC itself, a combined system of the SOFC with other power generation processes has been expected to be one of the most efficient power generation systems.

In a conventional fuel cell system, hydrogen as the preferred fuel is usually produced in an external reformer by the steam reforming of hydrocarbons such as methane or natural gas. Because the reforming reaction is endothermic which takes place at a high temperature over 800 K, the necessary heat can be supplied by combustion of a part of the fuel. On the other hand, heat discharged from the electrode of the SOFC is high enough in temperature to be supplied for the steam reforming. The reforming may then occur in the SOFC internally without the addition of any external reformer. Therefore, this type of SOFC, an internal-reforming SOFC (IR-SOFC), saves the energy of the fuel which might have been consumed in the external reformer and enables the energy conversion efficiency of its combined system be extremely high. Some calculations [1–3] revealed that a combined system of an IR-SOFC with a gas turbine or both gas and steam turbines would provide a power generation efficiency of over 65%.

In a direct IR-SOFC, steam reforming of methane takes place directly over the anode, thus anode material must be a suitable catalyst for the steam reforming. Regarding the advances in catalysts for the direct IR-SOFC, a recent review [4] may provide useful information. Ni–YSZ cermet, which is a conventional anode material, is a good catalyst for the steam reforming under appropriate conditions [5–11]. When the molar ratio of steam to methane in the reaction gas, S/C, is smaller than a certain value, carbon deposition occurs on the anode [12], and this may cause blocking of the pores in the porous electrode. To prevent the anode from carbon deposition, an addition of $CeO_2$ to the Ni–YSZ cermet can be effective [7,13]. When the partial pressure of hydrogen in the fuel is too small, the catalytic activity of the anode rapidly deteriorates [14]. This may be due to the oxidation of Ni in the relatively weak reducing atmosphere and at high temperature. This also suggests that the deterioration may be caused by high current-density operation because $H_2O$ is produced at the anode/electrolyte interface by the

* Corresponding author. Tel.: +81-277-30-1458; fax: +81-277-30-1457.
*E-mail address*: nakagawa@bce.gunma-u.ac.jp (N. Nakagawa).

0378-7753/01/$ – see front matter 
PII: S0378-7753(00)00508-5

electrochemical oxidation of hydrogen, which cannot be ignored because high current-density operation, over 0.3 A/cm$^2$, might be carried out in a practical SOFC.

For the direct IR-SOFC, it is important to investigate the catalytic activity of the actual anode, usually porous layer of Ni-composite coated on a zirconia electrolyte, not only on open circuit but also under closed circuit conditions. However, only a few reports dealt with the steam reforming over the anode in an actual SOFC. Then the catalytic activity of the actual anode under various conditions, like under current discharging, has not been made clear yet. To study the catalytic activity in detail, it is desirable to use a differential fuel cell reactor, through which reaction conversion is small.

In this paper, by introducing a gas mixture of methane and steam to a SOFC reactor directly, effect of gas compositions, temperature and the electrochemical oxidation by current discharging on the catalytic activity was investigated under the conditions where the reactor was operated as a differential reactor. The electrode material employed was Ni–YSZ–$CeO_2$ which may be a promising anode material for the direct IR-SOFC.

## 2. Experimental

The anode material used was Ni–YSZ (yttria-stabilized zirconia)–$CeO_2$, which was expected to enhance the reforming activity and stability with respect to carbon deposition [7,13]. In the preparation of the anode material, NiO powder, YSZ powder (TOSO, TZ-8Y $(ZrO_2)_{0.92}$ $(Y_2O_3)_{0.08}$) and $CeO_2$ powder (Wako Chem. Co. Ltd.) were weighed in a volumetric ratio of Ni:YSZ:$CeO_2$ equal to 50.0:37.8:12.2 and were ground using a high-speed vibrating mill (TI-100, Iwaki Factory). The volumetric ratio was determined from the previous studies of the Ni–YSZ anode [15] and the conductivity of the $ZrO_2$–$CeO_2$–$Y_2O_3$ system [16]. The mixture was heated at 1673 K for 4 h in air and then ground again then resulted in the average particle size of 0.5 μm. The mixed powder was suspended in turpentine oil and coated in the shape of rectangle, 5 mm×10 mm, on the surface of a solid electrolyte disk of 25 mm diameter and 200 μm thickness. The amount of the coated mixed-powder was 0.044 g/cm$^2$ with the electrode thickness about 110 μm. The solid electrolyte was 3 mol% yttria-doped zirconia. The coated disk was then baked at 1673 K for 4 h in air so that the coated layer became a porous coating used for the Ni–YSZ–$CeO_2$ anode. On another surface, Pt paste was coated and baked at 1273 K for 1 h and used as the cathode. A small Pt electrode was also placed at the periphery and used as the reference electrode.

The cell was placed in the high-temperature fuel cell setup shown in Fig. 1, and the configuration of the gas inlet tubes and the cell is shown in Fig. 2. A gas mixture of $CH_4$–$H_2O$–$H_2$–$N_2$ and air were vertically blown to the surface of the anode layer and the Pt cathode, respectively. The distance between the top of the gas inlet tube and the anode layer was set at about 5 mm. Since a small part of reactant gas may not contact with the electrode, a little reduced reaction-rate may be obtained from this type of reactor. However, dependencies of gas composition, temperature and current flow on the catalytic activity can be evaluated adequately under appropriate gas flow rates.

The feed rate of steam was controlled by a water feeding-pump connected to the steam generator. Gas components of $CH_4$, $H_2$, $N_2$, CO and $CO_2$ at the inlet and the outlet were analyzed by gas chromatography. From the change in the gas

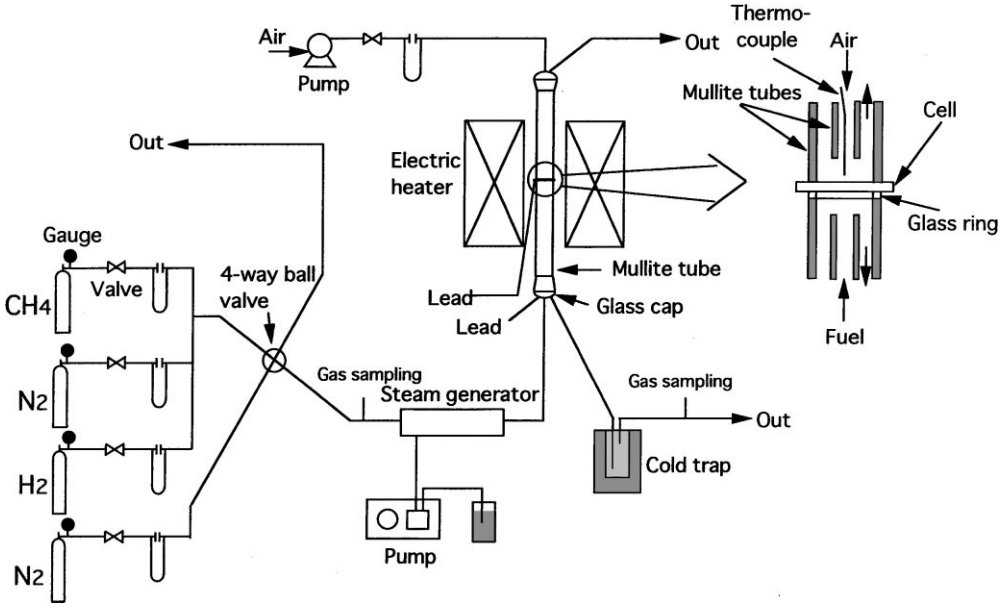


Fig. 1. Experimental setup of the internal steam-reforming fuel cell.

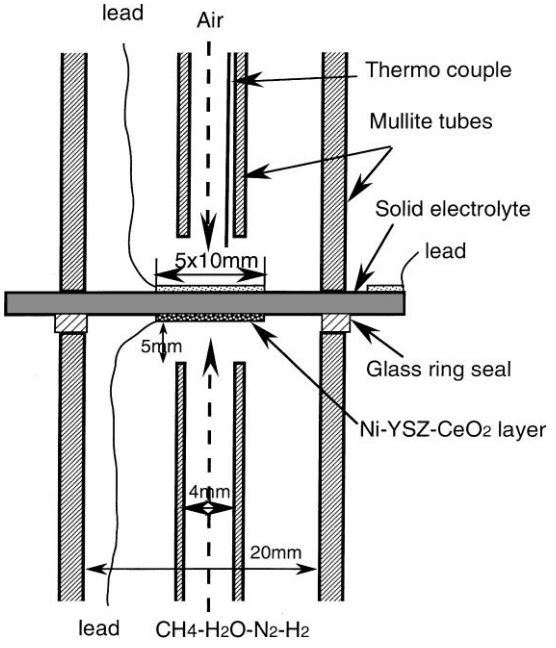


Fig. 2. Geometry of the gas inlet tubes and the electrodes in the differential fuel cell reactor.

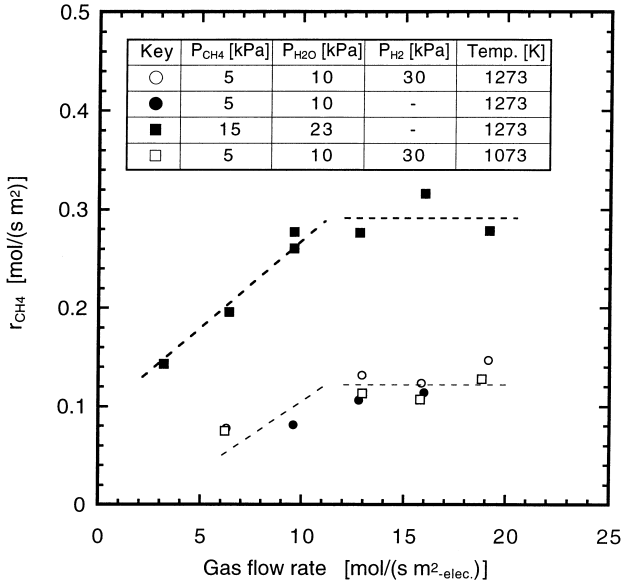


Fig. 3. Effect of gas flow rate on the reaction of steam reforming for the differential fuel cell reactor.

compositions between the inlet and the outlet, the production rate was calculated for CO, $CO_2$ and $H_2$ based on the gas flow rate and the apparent surface area of the anode:

$$r_i = \frac{F(X_{\text{out},i} - X_{\text{in,o}})}{A} \quad (1)$$

where $r_i$ (mol/($m^2$ s)) is the rate of the $i$ species, $F$ (mol/s) the gas flow rate, $x_i$ the molar fraction of $i$ and $A$ ($m^2$) is the apparent surface area of the anode.

On the other hand, the rate of steam reforming, i.e. the rate of methane consumption, was calculated from the sum of $r_{CO}$ and $r_{CO_2}$.

$$r_{CH_4} = -(r_{CO} + r_{CO_2}) \quad (2)$$

The conversion of $CH_4$ was at most 15%, and as shown in Figs. 11 and 12, the magnitude of $r_{CO_2}$ was much smaller compared to that of $r_{CO}$ suggesting that the water–gas shift reaction was negligible in this experiment.

The measurement of the reaction rates was conducted in the temperature range 973–1273 K and with a ratio of steam to carbon between 2 and 7. The anode potential on open circuit and the potential–current relationship on closed circuit were also measured in the usual way during the steam reforming over the anode.

## 3. Results and discussion

### 3.1. Effect of gas flow rate on the reforming rate

Fig. 3 shows effect of gas flow rate on the rate of steam reforming. As mentioned below, the catalytic activity of the anode gradually deteriorated at low partial pressures of hydrogen. The data shown in the figure were obtained at the initial activity that the deterioration was negligibly small. When the gas flow rate was below 12 mol/(s $m^2$-electrode), the reforming rate increased with increasing the gas flow rate suggesting that the mass transfer between the bulk gas and the anode surface is the rate determining. On the other hand, the reforming rate was almost constant in the range where the gas flow rate was over this value. In this range, the following experiments were conducted.

### 3.2. The rate of steam reforming of methane on open circuit

When the partial pressure of hydrogen in the reaction gas was below 5 kPa, the catalytic activity of the anode declined with time of exposure of the layer to the gas, which resulted in a drop in the reaction rate of the steam reforming. This may be caused by the oxidation of the Ni surface by steam at a lower pressure of hydrogen, because reaction rate was found restoring to the initial state by exposing the anode to hydrogen for a while. This suggests that a small amount of hydrogen should be included in the reaction gas to make the atmosphere reductive and keep the catalytic activity constantly high. In a practical case, a recycle of a small part of gas, from the outlet of the anode to its inlet, may be needed for the direct IR-SOFC system.

Thereafter, the experiments were conducted using a reaction gas with hydrogen at over 10 kPa. Fig. 4 shows the effect of the partial pressure of hydrogen on $r_{CH_4}$ The rate was not influenced by the partial pressure of hydrogen in this range.

Fig. 5 shows the effect of the partial pressure of $CH_4$, $P_{CH_4}$, on the rate of steam reforming on open circuit and at

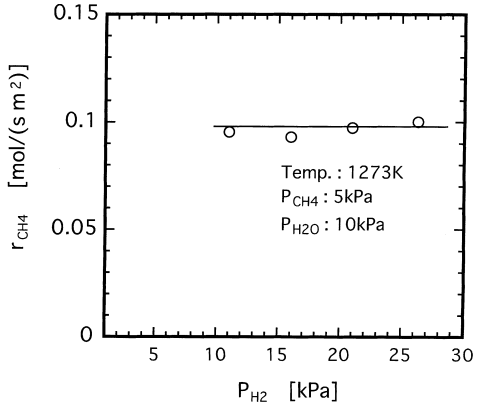


Fig. 4. Effect of partial pressure of hydrogen on the rate of the steam reforming when the partial pressure of hydrogen was over 10 kPa.

1073 K. It was found that the reaction rate increased with increasing $P_{CH_4}$ The dependency of $P_{CH_4}$ on $R_{CH_4}$ was nearly first order of $P_{CH_4}$ at low $P_{CH_4}$, whereas, it became smaller with increasing $P_{CH_4}$.

Figs. 6 and 7 show the effect of the partial pressure of $H_2O$, $P_{H_2O}$, on $r_{CH_4}$ at 1073 and 1273 K, respectively. The

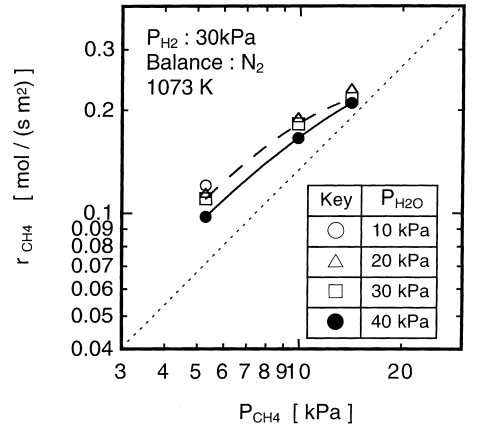


Fig. 5. Effect of partial pressure of methane on the rate of the steam reforming obtained at 1073 K.

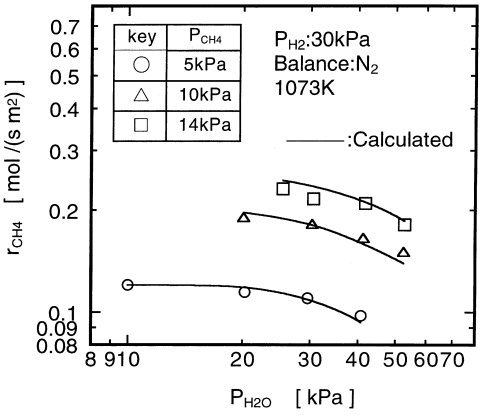


Fig. 6. Effect of partial pressure of steam on the rate of the steam reforming of methane obtained at 1073 K.

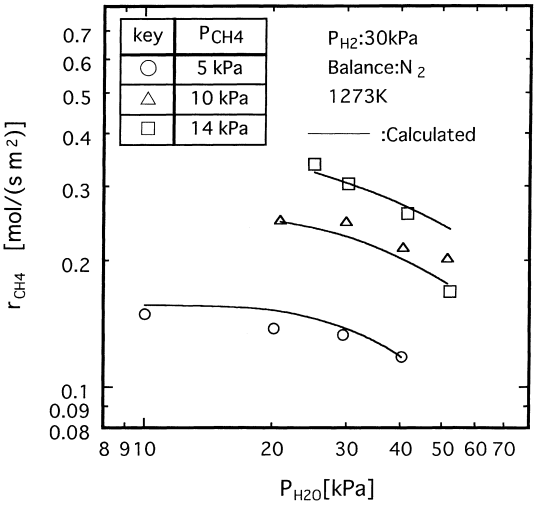


Fig. 7. Effect of partial pressure of steam on the rate of the steam reforming of methane obtained at 1273 K.

rate of steam reforming was almost independent of $P_{H_2O}$ at low $P_{H_2O}$ and low $P_{CH_4}$. However, the rate decreased with increasing $P_{H_2O}$ and $P_{CH_4}$. The solid lines in the figures are the calculated rates with an equation that will be proposed later. Similar dependencies of $P_{CH_4}$ and $P_{H_2O}$ on the rate were obtained at other temperatures between 973 and 1273 K. Such dependencies of $P_{CH_4}$ and $P_{H_2O}$ on $r_{CH_4}$ in this experiment are similar to the results reported so far, i.e. the rate was proportional to the first order of $P_{CH_4}$ [5,6], and between 0 and $-1$ order for $P_{H_2O}$ [6].

Fig. 8 shows the effect of temperature on the rate. As a reference, the reforming rate obtained from Ni–YSZ film [6] was shown by the dotted line. The apparent activation energy in this range for the Ni–YSZ–$CeO_2$ was 18 kJ/mol and is lower than that of Ni–YSZ film: 82 kJ/mol. On the other hand, it is noted that the catalytic activity of Ni–YSZ–$CeO_2$ was higher than that of Ni–YSZ especially at low temperature.

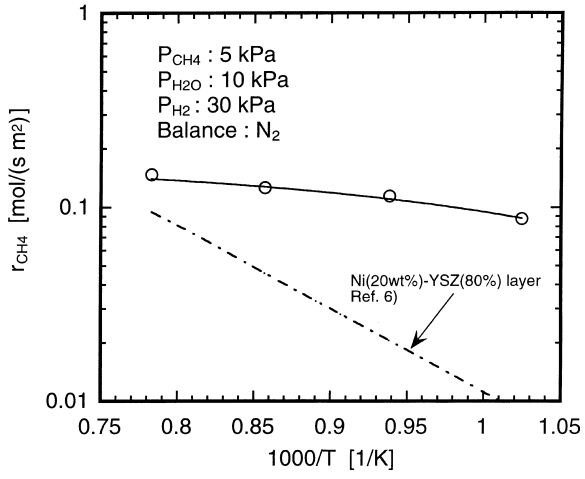


Fig. 8. Dependence of temperature on the rate of the steam reforming of methane.

To express the above effects of $P_{CH_4}$, $P_{H_2O}$ and temperature on $r_{CH_4}$ quantitatively, the following equation of a fractional expression was proposed as a result of adapting the data to various formulas of equation:

$$r_{CH_4}(\mathrm{mol/s\,m^2}) = \frac{K_1K_2K_3P_{CH_4}P_{H_2O}}{(1 + K_2P_{CH_4} + K_3P_{H_2O})^2}$$

$$K_i = A_i \exp\left(\frac{-E_i}{RT}\right), \qquad i = 1, 2 \tag{3}$$

where $A_i$ and $E_i$ are constants, $R$ the gas constant and $T$ is the temperature. This equation can be used to realize the reaction rate of the steam reforming at the initial stage that the rate of the shift reaction is negligible. Other application ranges of this equation are 5 kPa$<P_{CH_4}<$15 kPa, 10 kPa $<P_{H_2O}<$50 kPa, 10 kPa$<$ $P_{H_2}<$30 kPa, 975 K$<T<$1275 K. The solid lines in Figs. 5–7 show the reaction rates calculated from the equation employing the values of the kinetic parameters listed in Table 1. This shows that the measured rates are almost consistent with the calculated ones.

One may explain Eq. (3) based on the Langmuir–Hinshelwood model. In this case, the constant $K_2$ and $K_3$ correspond to the equilibrium constants for adsorption of $CH_4$ and $H_2O$ on the adsorption site of the catalyst, respectively. $K_3$ was calculated to be three to six times larger than $K_2$ in the range between 1000 and 1300 K. However, the positive value of the activation energy for the $H_2O$ adsorption, $E_3$, cannot be explained by the usual adsorption theory. This suggests that the mechanism is not so simple.

### 3.3. Anode potential and polarization

Fig. 9 shows the open-circuit voltage during the steam reforming which was taking place at the anode. The cell voltage, $E$, theoretically is related to the ratio of oxygen potentials between the anode and cathode according to the Nernst equation

$$E = -\left(\frac{RT}{4F}\right) \ln\left(\frac{P_{O_2,\mathrm{anode}}}{P_{O_2,\mathrm{cathode}}}\right) \tag{4}$$

where $F$ is the Faraday constant.

One can then calculate the oxygen potential of the anode by specifying air for the cathode. It has been known that the anode potential for a gas mixture consisting of $H_2$, $H_2O$, CO and $CO_2$ agreed with the value calculated by assuming that the oxygen potential was in equilibrium with the $H_2$–$H_2O$ in the mixture. The triangles and squares in the figure show the calculated voltages by assuming that the anode oxygen potential was in equilibrium with $H_2$–$H_2O$ and CO–$CO_2$ of the outlet gas, respectively. Whereas, the solid line shows the calculated voltage by assuming that both the steam reforming and the shift reaction equilibrated at this temperature. The measured voltages agreed with the solid line suggesting that those reactions reached equilibrium at the anode/electrode interface where the anode potential was detected. From the figure, one may deduce that there was a difference in gas composition between the anode surface and the bottom of the anode, i.e. anode/electrolyte interface.

Table 1
Kinetic parameters determined for Eq. (3) in this experiment

| $i$ | $A_i$ | $E_i$ (kJ/mol) |
|---|---|---|
| 1 | 400–612 mol/(s m$^2$) | 49 |
| 2 | $3.01 \times 10^{-4}$–$4.96 \times 10^{-4}$ (kPa)$^{-1}$ | −45 |
| 3 | 0.18–0.28 (kPa)$^{-1}$ | 7 |

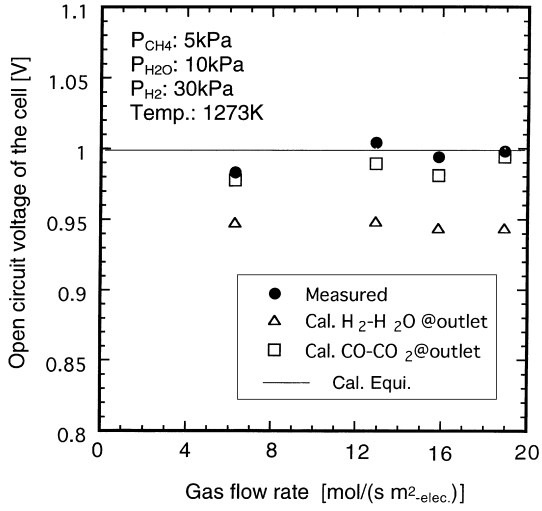


Fig. 9. Open circuit voltages of the cell measured and simulated.

When the circuit is closed, electrochemical oxidation of the reforming products, $H_2$ and CO, occur at the three-phase zone, gas/electrode/electrolyte interface which is considered to be a substantial reaction zone and at which $H_2O$ and $CO_2$ must be produced. Hydrogen would mainly be consumed by the electrochemical oxidation, because hydrogen was predominantly oxidized in the $H_2$–CO mixture at the anodic reaction [17] and also the fraction of CO in the mixture was much lower than that of $H_2$. Fig. 10 shows the relationships between current and the anode potentials under the reforming condition and the $H_2$–$H_2O$ gas mixtures that were prepared to simulate the reforming gas. Methane itself in the reaction gas acts as an inert gas at the anode potential [17]; therefore, a $H_2$–$H_2O$ mixture shown as the squares was used to simulate the gas mixture at the anode/electrolyte interface on open circuit. Another $H_2$–$H_2O$ mixture, as the triangles, was used to simulate the outlet gas. The measured potentials appeared between the plots for the simulated gases. Namely, the measured potential was equal to the square plot on open circuit and left the curve of the square plots over 50 mA/cm$^2$, then get close to the line of the triangle plots with increasing current density and finally almost agreed with the triangle plots over 600 mA/cm$^2$. This figure suggests that the reforming reaction taking place in the pores of the anode influenced the anode potential.

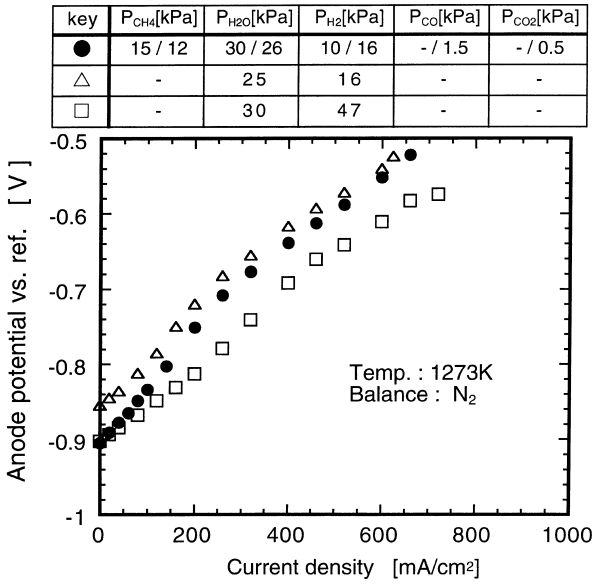


Fig. 10. Relationships between the anode potential and current density obtained from the reforming gas and $H_2$–$H_2O$ gas mixtures used to simulate the reforming gas.

### 3.4. Effect of current flow on the catalytic activity for the steam reforming

Fig. 11 shows the reaction rates not only for $CH_4$ but also for $H_2$, CO and $CO_2$ measured with increasing current density at $P_{CH_4}$=6 kPa, $P_{H_2}$=30 kPa and $P_{H_2O}$=18 kPa. The reaction rates were measured after continuing the current discharge for about 1 h. The reaction products of the steam reforming, hydrogen in this case, were consumed by the electrochemical oxidation; therefore, the measured rate was the overall rate that involves formation by the reforming reaction and consumption by the electrochemical oxidation. The overall rate of hydrogen with current density

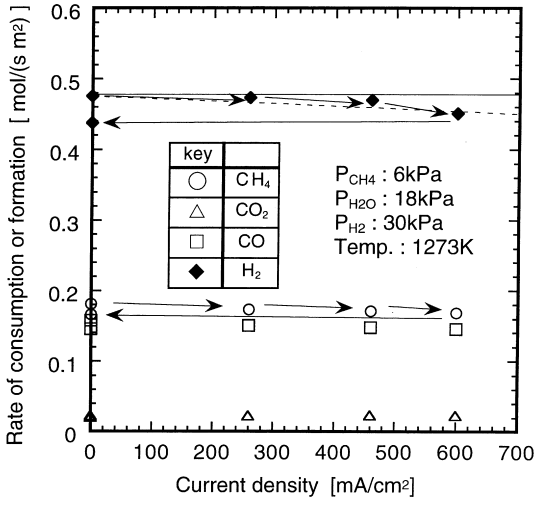


Fig. 11. Effect of current density on the rate of the reactions when the partial pressure of steam was relatively low: 18 kPa.

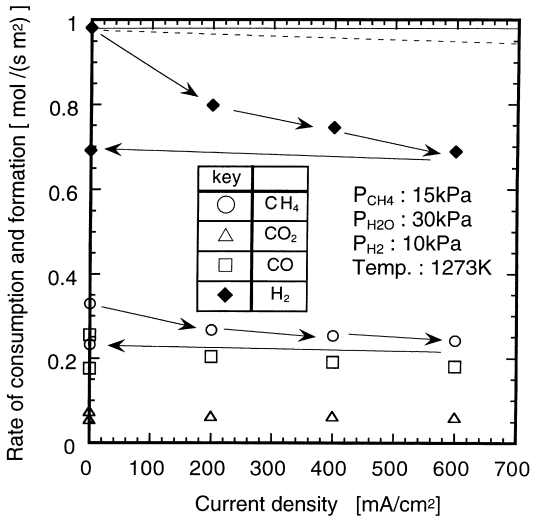


Fig. 12. Effect of current density on the rate of the reactions when the partial pressure of steam was relatively high: 30 kPa.

was calculated and is shown as the dotted line. The overall rate of $H_2$ formation was found to decrease with increasing current along the dotted line, suggesting that the overall rate can be explained by the sum of the reforming rate and the consumption rate.

It is noted that when the circuit was opened again after the current discharge of 600 mA/cm$^2$, the catalytic activity was not back to the initial value and the rate remained as that at 600 mA/cm$^2$. This suggests that the catalytic activity deteriorated during a current load as high as 600 mA/cm$^2$. Much greater deterioration of the catalytic activity during current discharge was observed at higher $P_{H_2O}$ and lower $P_{H_2}$. Fig. 12 shows the rates with increasing current obtained at $P_{CH_4}$=15 kPa, $P_{H_2}$=10 kPa and $P_{H_2O}$=30 kPa. The decrease in the rate of $H_2$ formation during current discharging was much larger than the calculated value shown by the dotted line, and also the rate was not back to the initial value after the circuit was opened in this case. However, the catalytic activity relieved after exposing the anode in a flow of hydrogen for a while. This suggests that the deterioration in the catalytic activity may be due to $H_2O$ produced via the electrochemical oxidation of hydrogen. This may be supported by the study of Nagata and Iwahara [18]. They measured the vapor pressure of $H_2O$ at the surface of a Ni–YSZ anode and concluded that the overvoltage at the anode was caused by hydrogen concentration polarization. Accumulated $H_2O$ in the porous anode may cause the oxidation at the Ni surface and resulted in the declaration. This effect would be influenced by the magnitude of the current density, the partial pressures of steam and hydrogen, and the structural factors of the anode, i.e. porosity, pore size, thickness and so on. In the design of the anode for the IR-SOFC, microstructure for higher mass transfer rate may be important from the viewpoint of preventing the catalytic activity from deteriorating.

## 4. Conclusions

The catalytic activity of a Ni–YSZ–$CeO_2$ anode layer of an IR-SOFC for the steam reforming of methane and the effect of the electrochemical oxidation on the activity were measured at various gas compositions between 973 and 1273 K, and the following conclusions were obtained:

1. The catalytic activity of the Ni–YSZ–$CeO_2$ anode was higher than that of the Ni–YSZ reported especially at low temperature as long as the reaction gas contains some hydrogen.
2. The rate of methane consumption over the anode in this experiment was expressed as Eq. (3).
3. A gradual deterioration of the catalytic activity of the anode was observed at low $P_{H_2}$ and high $P_{H_2O}$ atmosphere, also at high current densities. This may be caused by the oxidation of Ni surface by steam with high $P_{H_2O}$ in the reaction gas and that produced via the electrochemical oxidation.

## References

[1] S. Nagata, A. Momma, T. Kato, Y. Kasuga, Extended abstracts, in: Proceedings of the Seventh Symposium on Solid Oxide Fuel Cells, Japan, December 1998, The Solid Oxide Fuel Cell Society of Japan, pp. 39–42.
[2] N. Mori, in: Proceedings of the 38th Meeting of the Solid Oxide Fuel Cell Society of Japan on Meeting Material, Tokyo, Japan, May 1999.
[3] M.R. Spakovsky, B. Olsommer, in: M. Ishida et. al. (Eds.), Proceedings of ECOS'99 on Efficiency, Costs, Optimization, Simulation and Environmental Aspects of Energy Systems, Tokyo, Japan, pp. 100–104.
[4] S.H. Clarke, A.L. Dicks, K. Pointon, T.A. Smith, A. Swann, Catal. Today 38 (1997) 411–423.
[5] A.L. Lee, R.F. Zabransky, W.J. Huber, Ind. Eng. Chem. Res. 29 (1990) 766–773.
[6] E. Achenbach, E. Riensche, J. Power Sources 51 (1994) 283–288.
[7] V.D. Belyaev, T.I. Politova, O.A. Mar'ina, V.A. Sobyain, Appl. Catal. A: Gen. 133 (1995) 47–57.
[8] K. Eguchi, Y. Kunisa, M. Kayano, K. Sekizawa, S. Yano, H. Arai, Denki Kagaku 64 (1996) 596–601.
[9] H. Horita, N. Sakai, T. Kawada, H. Yokokawa, M. Dokiya, J. Electrochem. Soc. 143 (1996) 1161–1168.
[10] J. Meusinger, E. Riensche, U. Stimming, J. Power Sources 71 (1998) 315–320.
[11] A.L. Dicks, J. Power Sources 71 (1998) 111–122.
[12] C.M. Finnerty, N.J. Coe, R.H. Cunningham, R. M Ormerod, Catal. Today 46 (1998) 137–145.
[13] Q. Zhuang, Y. Qin, L. Chang, Appl. Catal. 70 (1991) 1–8.
[14] M.J. Saeki, H. Uchida, M. Watanabe, Catal. Lett. 26 (1994) 149–157.
[15] N. Nakagawa, K. Nakajima, M. Sato, K. Kato, J. Electrochem. Soc. 145 (1999) 1290–1295.
[16] B. Cales, J.F. Baumard, J. Electrochem. Soc. 131 (1984) 2407–2413.
[17] T. Kawada, I. Anzai, N. Sakai, H. Yokokawa, M. Dokiya, High temperature electrode materials and characterization, D.D. Macdonald, A.C. Khandkar (Eds.), The Electrochemical Society Proceedings Series, Pennington, NJ, PV 91–6, 1991, p. 165.
[18] N. Nagata, H. Iwahara, J. Appl. Electrochem. 23 (1993) 275–278.